SAND2014-18744J

Parallel Operation of Multiple Closely Spaced Small Aspect Ratio Rod Pinches

Victor J. Harper-Slaboszewicz, *Member*, *IEEE*, Joshua Leckbee, Nichelle Bennett, Elizabeth A. Madrid, David V. Rose, Carsten Thoma, Dale R. Welch, Patrick W. Lake, and Andrew L. McCourt

***Abstract*—A series of simulations and experiments to resolve questions about the operation of arrays of closely spaced small aspect ratio rod pinches has been performed. Design and post-shot analysis of the experimental results are supported by 3D particle-in-cell simulations. Both simulations and experiments support these conclusions. Penetration of current to the interior of the array appears to be efficient, as the current on the center rods is essentially equal to the current on the outer rods. Current loss in the feed due to the formation of magnetic nulls was avoided in these experiments by design of the feed surface of the cathode and control of the gap to keep the electric fields on the cathode below the emission threshold. Some asymmetry in the electron flow to the rod was observed, but the flow appeared to symmetrize as it reached the end of the rod. Interaction between the rod pinches can be controlled to allow the stable and consistent operation of arrays of rod pinches.**

***Index Terms*—rod pinch**

I. Introduction

The rod pinch diode [1] is used for high-brightness x-ray radiography by many pulsed-power accelerators [2]. It is composed of an anode rod that is attached to a planar anode and extends through a washer-shaped cathode plate. An electron beam is initiated by field emission from the edges of the cathode hole. The cathode plasma formed at the emission points spreads over the cathode surface, so the electron beam flows from a plasma cathode covering the cathode surface. The current is space-charge-limited and forms a weak pinch under the influence of the magnetic field generated by the electron flow. This beam heats the anode rod and creates a surface plasma. Plasma ions are drawn out of this plasma and counterstream toward the cathode creating a bipolar flow. The space-charge of the ions partially neutralizes that of the electrons which increases the current density and enables the beam to become tightly pinched. The impedance behavior of this flow has been well characterized [3][EM1] for radiography rod pinches operated at impedances of 10-50 ohms or higher.

Rod pinches have many desirable operational characteristics, including simplicity of fabrication, stable operation, and high areal current density. This work is directed toward applying these desirable characteristics to diodes for low impedance pulsed power drivers. The plasma-filled rod pinch has previously been investigated as a method of obtaining low impedance operation [4][EM2]. Another method for obtaining the desired low impedance is to operate multiple rod pinches in parallel, as well as operating those rod pinches at small aspect ratio [5]. To maintain the high areal current density, the rod pinches should be closely spaced. This type of diode geometry for a low impedance driver has not been previously investigated.

This work describes simulations and experiments to evaluate the effectiveness of a technique to mitigate concerns about coupling between multiple closely coupled small aspect ratio rod pinches. These experiments use a 3 Ω Linear Transformer Driver (LTD) based on part of the flash radiography research source URSA Minor [5].

A. Concerns for closely-coupled rod pinches

There are several concerns for multiple closely spaced rod pinches. These include penetration of the current to the interior of the rod pinch array, loss of magnetic insulation in the feed, and asymmetry in the rod pinch flow.

The concern about penetration of the current to the interior of the array is related to the concept of skin depth, and is based on the higher path resistance and inductance to the diodes in the interior of the array. This higher path inductance reduces the voltage on the inner diodes, so the outer diodes should begin conducting before the inner diodes. Once they begin to conduct, the impedance of the array drops, further reducing the voltage available to start conduction on the inner diodes. It is possible that as a result the inner diodes would

Submitted for review September , 2014. This work was supported by the Laboratory Directed Research and Development (LDRD) program at Sandia National Laboratories. Sandia National Laboratories is a multi-program laboratory managed and operated by Sandia Corporation, a wholly owned subsidiary of Lockheed Martin Corporation, for the U.S. Department of Energy's National Nuclear Security Administration under contract DE-AC04-94AL85000.

V. J. Harper-Slaboszewicz is with Sandia National Laboratories, Albuquerque, NM 87185 USA (e-mail: vjharpe@sandia.gov).

J. Leckbee is with Sandia National Laboratories, Albuquerque, NM 87185 USA (e-mail: jjleckb@sandia.gov).

Nichelle Bennett is with National Security Technologies, LLC, Las Vegas, NV 89193 USA (e-mail: nlbenne@sandia.gov).

Elizabeth A. Madrid, David V. Rose, Carsten Thoma, and Dale R. Welch are with Voss Scientific, LLC, Albuquerue, NM 87111 USA.

P. W. Lake is with Sandia National Laboratories, Albuquerque, NM 87185 USA (e-mail: pwlake@sandia.gov).

A. L. McCourt is with Sandia National Laboratories, Albuquerque, NM 87185 USA (e-mail: almccou@sandia.gov).

just never start conducting.

The concern about loss of magnetic insulation in the feed is related to concerns for post-hole convolutes in vacuum magnetically-insulated transmission lines [6], although in rod pinches electron flow across the gap near the rod is intentional. Coupling of the magnetic fields from the multiple rods can result in magnetic nulls in the feed gap as shown in Fig. 1, which can result in current losses in the feed gap if electrons are in the gap and can reach the magnetic field nulls. Although the precise geometry of the magnetic field null depends on the details of the configuration, any closely spaced multiple rod pinch geometry will have magnetic field nulls somewhere between the rods.

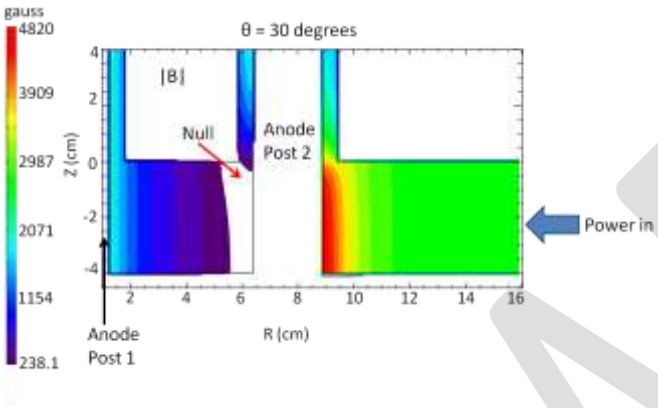

Figure 1 Magnetic field intensity in the feed gap for a multiple rod pinch configuration.

The concern about asymmetry in the electron flow is illustrated in Fig. 2, which shows the magnetic field at peak power based on simulations of a three rod geometry. The figure shows that there is considerable asymmetry in the magnetic field around the rod, particularly in the feed gap between the anode base plate and the cathode plate, which could perturb the electron flow and negatively affect the rod pinch operation.

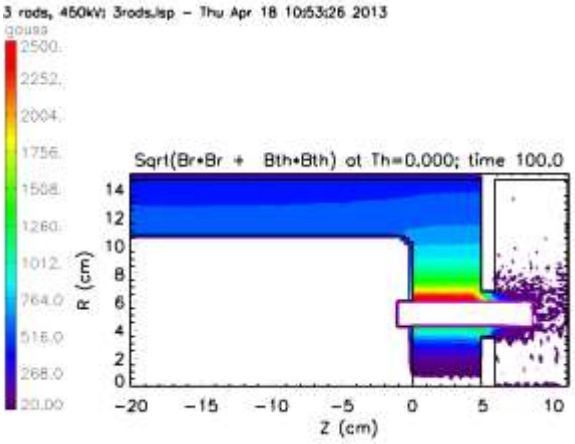

Figure 2 Magnetic field at peak power for a three rod configuration.

Initial evaluation of these concerns identified the following path forward. For the concern of current penetration to the interior of the diode array, the expectation was that, for a relatively long rise time source such as is used in these experiments, the issue would not arise. However, simulations and experiments with a diode array consisting of ten closely spaced small aspect ratio rod pinches were planned to allow verification that this issue was not significant. For the concerns about magnetic nulls in the feed and flow asymmetry about the rod, two mitigation approaches were identified. First, the rods can be partially isolated by surrounding each with a conducting hollow cylinder connected to the cathode plate, to reduce the magnetic field from adjacent rods in the vicinity of the rod. This approach was first successfully tested using simulations. Second, the cathode plate can be shaped to suppress field emission in the feed gap. These approaches were implemented and characterized in the ten rod pinch experiment, and supporting simulations using the experiment geometry were performed.

II. SIMULATIONS

All simulations were performed using the LSP code [7], which was used in a 3D, fully electromagnetic, fully kinetic, PIC mode.

A. Initial simulations

To evaluate the potential effects of magnetic field coupling between rod pinches on the electron flow, initial simulations were performed using the geometry of Fig. 3. This uses the simplest rod pinch geometry, in which the cathode is just a plate.

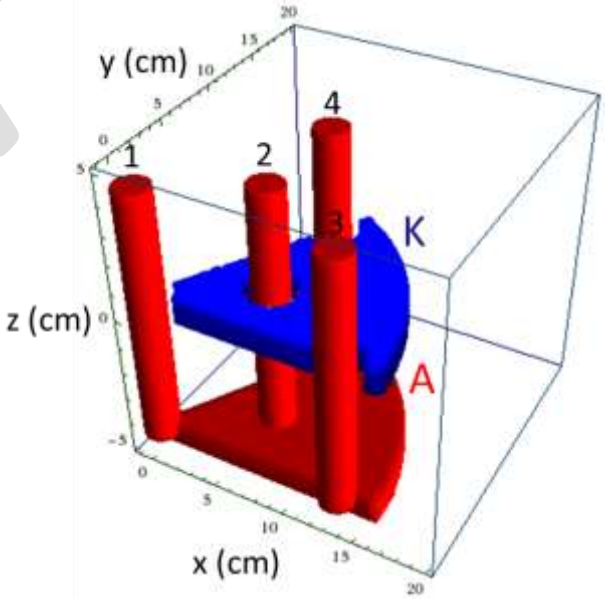

Figure 3 Geometry of initial simulations to evaluate magnetic field coupling effects in rod pinch diode arrays. 60 degree segment of hex lattice (rod on axis) with 6-fold symmetry.

First, an LSP simulation with no particles and resistive loads at the diodes showed substantial magnetic field asymmetry about the outer rods. The magnitude of the magnetic field just above the anode base plate is shown in

Fig. 4. The ratio of the magnetic field away from the axis to the field toward the axis on the outer rods is 2 to 3 for the outer ring of rods, and larger for the inner ring. The magnetic field in the feed gap between the rod and the axis is quite low, so electrons emitted in the A-K gap may not be fully confined by the magnetic field, and could flow into that gap.

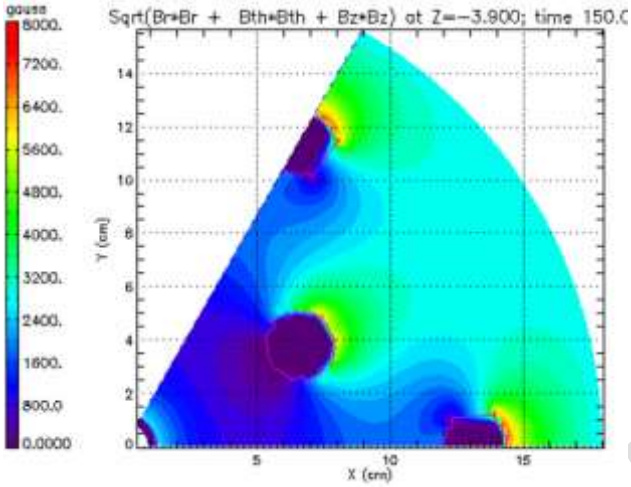

Figure 4 Magnetic field magnitude 1 mm above the anode baseplate for the rod pinch array geometry of Fig. 3.

This is illustrated in Fig. 5, which shows a simulation using the same geometry in which electron and ion emission were allowed. A realistic power pulse was used to drive the simulation. Classic rod pinch behavior of the ions and electrons is observed on the rod surface facing away from the axis, with the particles primarily present in the A-K gap and along the rod above the cathode plane. However, on the rod surface at small radius, electrons and ions stream into a region of low magnetic field in the feed gap between the rod and the axis.

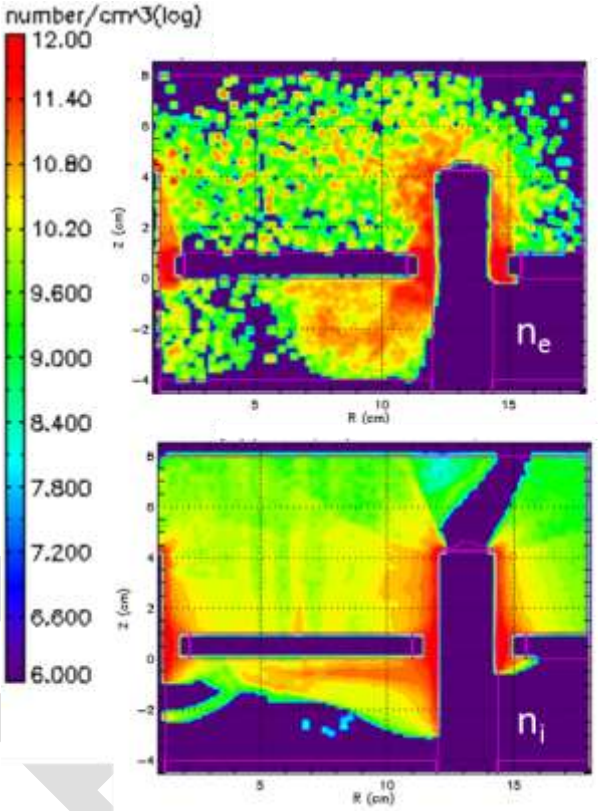

Figure 5 Electron and ion positions at peak power in the rod geometry of Fig. 3, viewed in the z-x plane with axis to the left.

One method of mitigating the effect of the weak magnetic field in the feed gap between the axis and the off-axis rod is to place a conducting cylinder around the rod, extending both above and below the cathode plate, that localizes and hence increases the magnetic field near the electron flow across the A-K gap. This would prevent streaming of electrons and ions from the A-K gap into the feed gap. The effect of such a conducting cylinder is shown in Fig. 6. This shows the results of a simulation using the same parameters as were used for Fig. 5, except that conducting cylinders extending to 2 cm above the anode baseplate were added around each rod. With these added cylinders, classic rod pinch behavior is observed on the on-axis and off-axis rods, and electrons and ions do not stream into the feed gap.

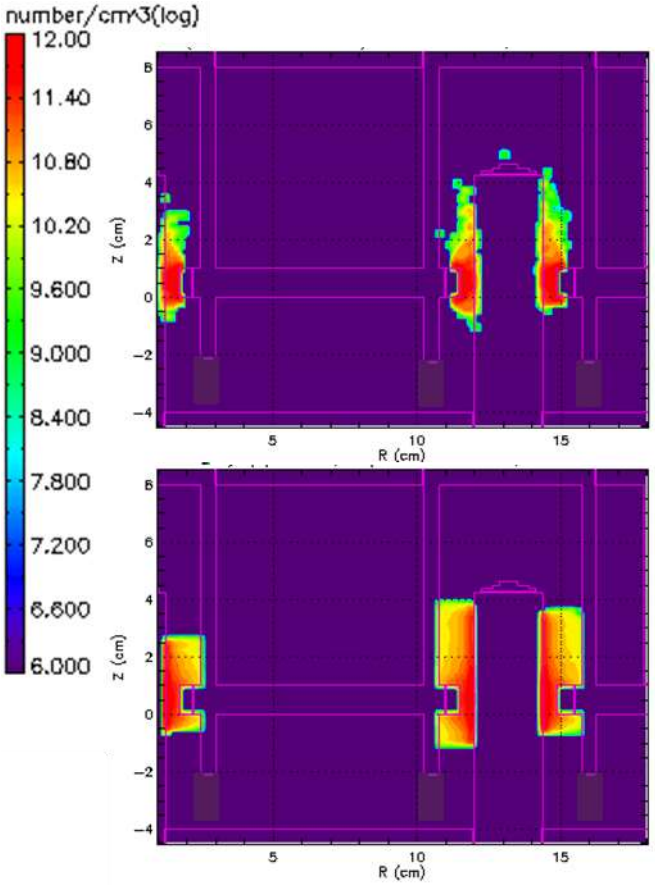

Figure 6 Electron and ion positions at peak power in the rod pinch geometry of Fig. 3, with partial conducting cylinders added around each rod.

B. Experiment simulation description

Asimulation of the 10-rod diode fielded on URSA Minor was built in Cartesian coordinates (x, y, z) which spans approximately 15 cm in the x- and y-directions and 40 cm in the z-direction. The simulation grid is comprised of nearly 7 million cells that range from 1 mm to 1.25 mm in the x- and y-directions and from 1 mm to 3 mm in the z-direction. The forward traveling voltage pulse used to drive the simulations reaches roughly 700 kV in approximately 90 ns as seen in Fig.7.

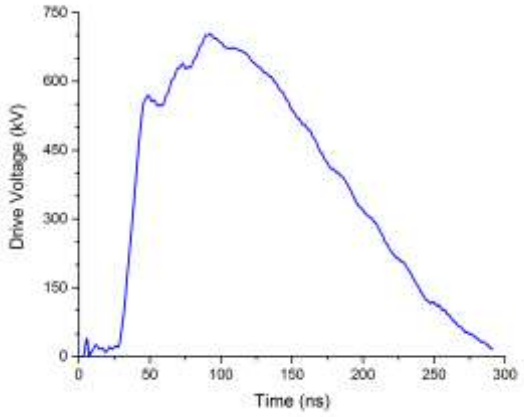

Figure 7 Drive voltage pulse assumed in simulations.

The solid tungsten anode rods are 1.2 cm in diameter, 7.5 cm in length, and are modeled within LSP using a Monte Carlo transport algorithm[8], [9]. Each rod and corresponding cathode hole has an AK gap of approximately 7 mm. Table 1 summarizes key dimensions for these simulations.

Table 1 Nominal geometric dimensions for simulation.

Variable	Description	Nominal Value
g_{AK}	Rod AK gap	0.7 cm
z_{pf}	Power flow gap	3.3 cm
z_{window}	Gap between rod tips and polycarbonate window	22.8 cm
d_{rod}	Rod diameter	1.2 cm

Fig. 8 shows a cut-away view of the simulation geometry in the top frame and a 2D view of the y-z plane marked with relevant dimensions in the bottom frame. Anode structures are in blue with tungsten rods in light blue, cathode structures are in red, and the polycarbonate window is in yellow.

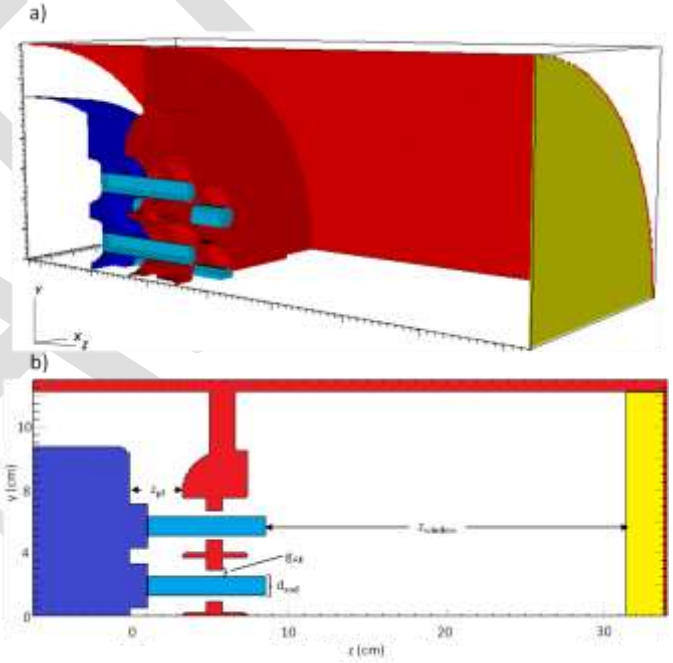

Figure 8 a) 3D simulation geometry shows one quarter of a 10-rod configuration. b) 2D view of the y-z plane at x=0.

Fig. 9 shows an x-y plane view of the anode rods and AK gaps in the center of the cathode plate. This view shows the stairstep structure of the holes and rods as well as the numbering scheme used to identify individual rods in both experiments and simulations. Note that the simulated diode encompasses a 90 degree segment of the full geometry and uses symmetry boundaries.

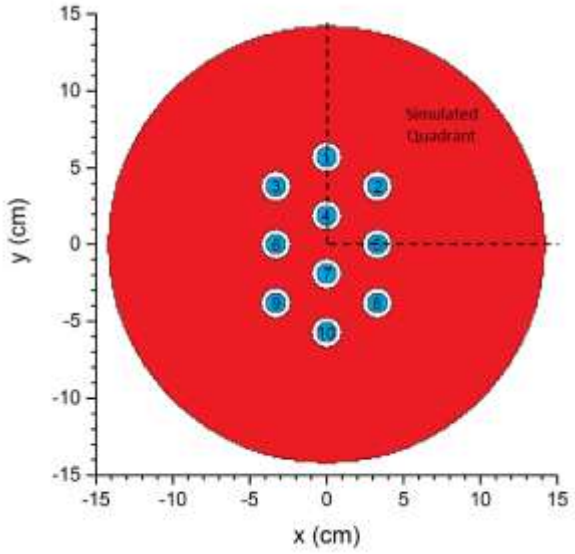

Figure 9 A view of the x-y axis in the center of the cathode plate (red) showing the positions and designated numbers for each rod (blue) in the simulation.

The cathode plate is designed in such a way that the cathode extends for roughly 4 cm along the length of each rod to provide the current path isolation discussed above.

Four different particle creation models were used in these simulations. Space charge limited electron emission was enabled for all cathode surfaces with an electric field stress greater than 250 kV/cm [10]. Electrons heat anode surfaces when they strike and deposit energy. This heating due to electron bombardment, along with Ohmic heating of the anode conductor, and can result in plasma formation and ion emission. This effect is included in the simulation model by allowing ion emission from anode surfaces that undergo a 400 K temperature increase [11]. Photons and electrons emitted from the tungsten rods are created based on electrons striking the rod. Fig. 10 shows the regions where each creation model is enabled in the simulation. Red outlines areas where anode ion emission can occur. Blue outlines areas where secondary electron and bremsstrahlung emission from the tungsten rods can occur. Green outlines areas where cathode electron emission can occur.

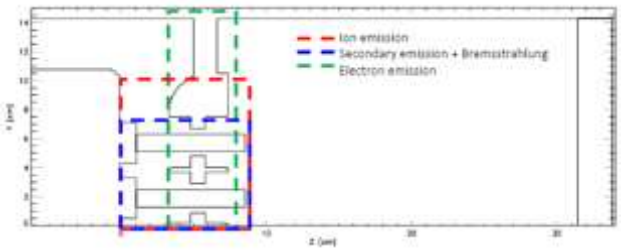

Figure 10 Two dimensional, y-z plane at x=0 of simulation space indicating particle creation regions.

Although the model includes electron and ion emission, it does not include the formation of dense electrode plasmas on the cathode and anode surfaces, which can then expand into the A-K gap, resulting in time-dependent closure of the gap and a consequent impedance collapse [12], [13].

C. Experiment simulation results

The simulated current as a function of time is shown in Fig. 11, which shows the current on rod 2, and the total 10-rod current, which is calculated by taking the average of the four rod currents in the simulation and multiplying by 10. The currents are not perfectly symmetric, since the peak current on rod 2 is about 13 kA, while the total current is 140 kA, so the outer rod carries a little less than one-tenth of the current. However, there is little variation in the currents among the 10 rods.

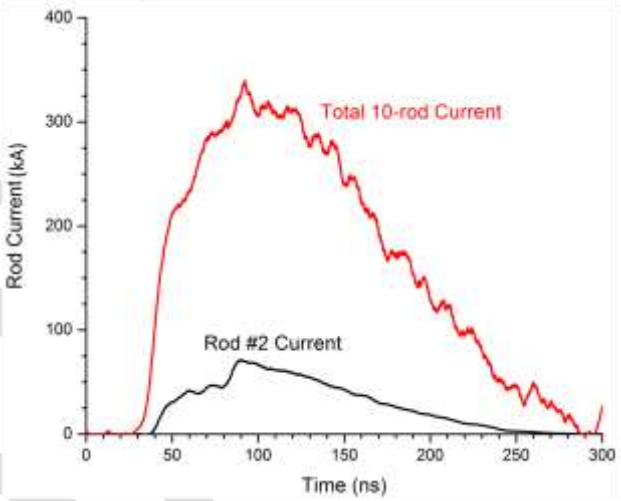

Figure 11 Current time history from simulation.

The simulated voltage as a function of time for the 4 rods is shown in Fig. 12. The voltage on rod 1, at the largest radius, rises fastest, and the voltage on rod 4, at the smallest radius, rises slowest, but the differences are small, and through most of the pulse the voltages on the 4 rods are very similar.

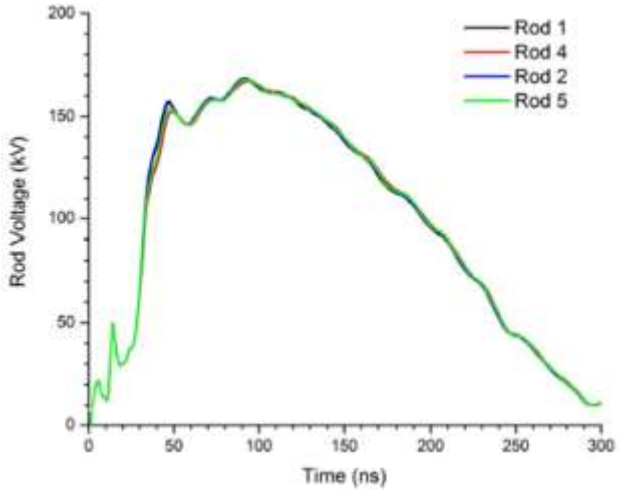

Figure 12 Rod voltage time histories.

Contours of the magnetic field are shown in Fig. 13 near the feed edge of the cathode plate at z=3.4 cm on the left and at the midplane of the cathode plate at z=5.3 cm on the right. Note the large asymmetry in magnetic field along each of the

rods near the end of the cathode plate. This asymmetry is largely eliminated by the midplane of the cathode as the fields from the currents on the other rod are largely shielded by the conducting cylinder along the rod provided by the shaping of the cathode plate.

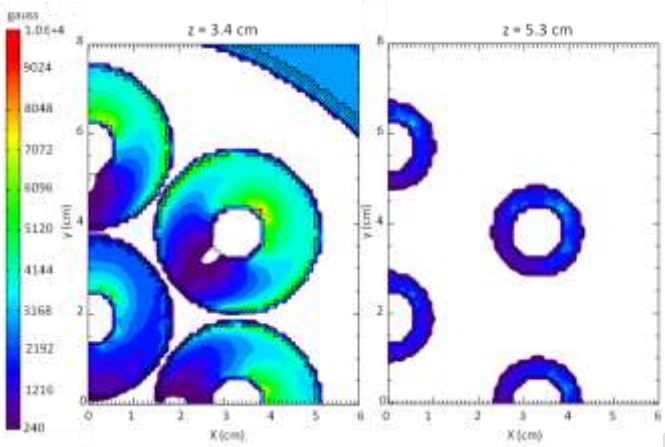

Figure 13 Magnetic fields at two locations in the diode show the nonuniform magnetic field along the rod.

The diode impedance calculated from these currents and voltages is shown in Fig. 14. Note that it reaches a minimum value of about 1.2 ohms and then increases later in time. It does not show a collapse in impedance late in time as the electrode plasmas close the A-K gap in the experiment.

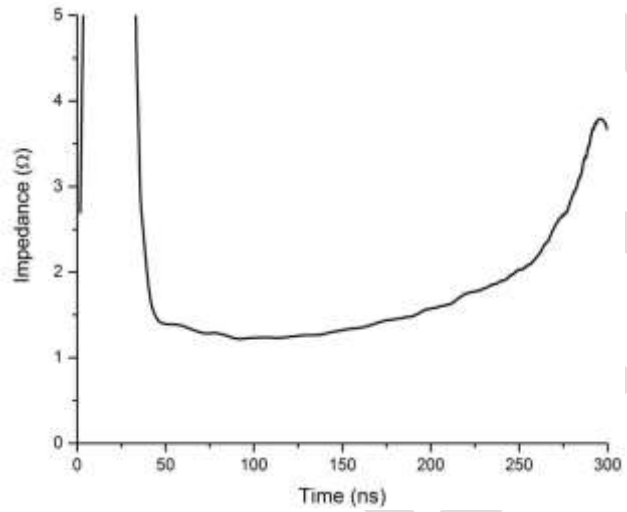

Figure 14 Diode impedance from simulations.

Electron and ion positions at t=150 ns are shown in Fig. 15. Note that the electron density is higher on the axis-facing surface of the outer rod. Electron emission from the corners of the cathode extensions is minimal and ion emission from the base of the rods is nonexistent. These results are consistent with the preliminary simulations shown in Fig. 6.

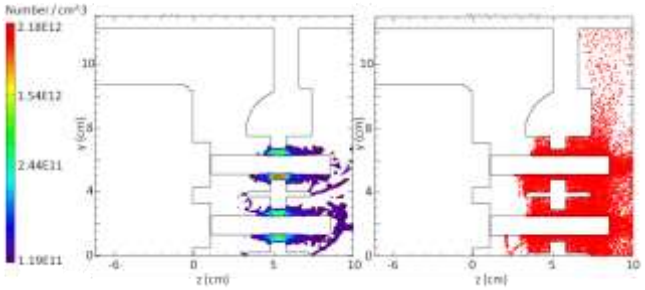

Figure 15 Electron density (left) and ion particle positions (right) at 150 ns.

Energy deposition along the rod was calculated from the electron deposition and is shown in Fig. 16. A dark band near the cathode is visible indicating an area of high electron bombardment of the rod. As is clear from both the electron densities in Fig. 15 and the energy deposition in Fig. 16, the pinch does not move strongly along the rod, and the bulk of the flow is in and near the A-K gap.

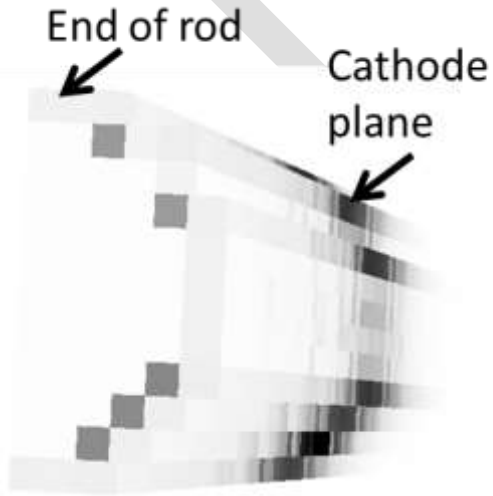

Figure 16 Simulated energy deposition along rod 4. This figure shows half the rod. The viewing angle is about 10 degrees from the system axis, and is similar to that in Fig. 22.

III. Experiments

A. *Experiment description*

URSA Minor was operated in positive polarity with a shortened anode stalk, with five LTD cavities. The cavities were charged to 75 kV. The anode stalk diameter was 21.5 cm, and the inside diameter of the cathode line was 29 cm. A pattern of 10 tungsten rods, with radius 0.635 cm, in a hexagonal closely packed configuration was mounted on the end of the anode stalk. The radius of the cathode holes was 1.27 cm, and the width of the cathode rings was 1 cm. Fig. 17 is a sketch of this configuration.

The design feed gap between the edge of the Rogowski coil holder at the base of each rod and the closest point on the cathode plate was 1.3 cm. In the first set of experiments, that gap was set at 0.4 cm. After the first few shots, the gap was increased to 1.4 cm.

The rods protruded 3 cm beyond the cathode plate. A

vacuum region extended axially 21 cm beyond the cathode plate, with an inside diameter of 21.3 cm. At the end of the vacuum region, a 2.73 cm thick polycarbonate window with the same diameter as the vacuum region allowed optical inspection of the alignment of the anode to the cathode hole.

Two PIN diodes were fielded on axis 33 cm from the outside of the window to measure the radiation pulse shape. CaF_2:Mn thermoluminescent dosimeters (TLD) 0.9 mm thick equilibrated by 0.25 mm of aluminum were used to characterize the radiation environment produced by the rod pinch. A pattern of nine TLDs, with one on axis, four at 3 cm radius, and four at 6 cm radius was fielded on the outside of the window.

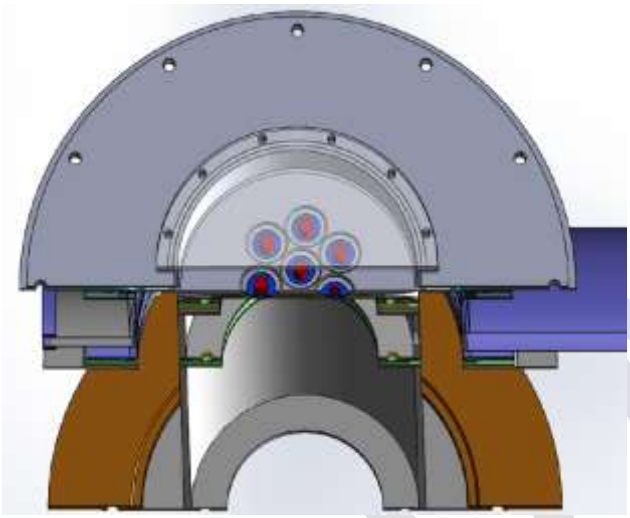

Figure 17 Cutaway sketch of diode region for 10 rod experiments.

Calibrated current diagnostics were mounted in the machine at 5 axial locations along the cathode and anode. At each position, either 2 or 4 B-dot probes or Rogowski coils were mounted to measure the current. The current measurement position closest to the diode load was just at the end of the anode stalk. Self-integrating Rogowski coils on the base of the anode rods labeled RODROG provided an additional measure of rod current. The Rogowski coils were nominally identical in construction. However, when they were individually calibrated prior to the series, there was significant scatter in the calibrations. The diagnostic positions closest to the diode are shown in Fig. 17.

In addition, capacitive V-dot probes were located on the inner and outer lines at the D and E positions, labeled IDV90 and IEV90, respectively. The V-dot probes used these experiments were calibrated in position using reference resistive voltage monitors. These voltage signals were inductively corrected to the rod position using the IEB0 (the B-dot on the inner line at the E position close to the end of the anode stalk) current signal and the calculated inductance from the current monitor to the outer radius of the rod pattern.

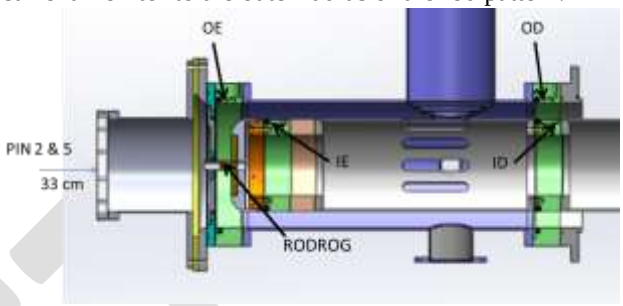

Figure 18 Diagnostic positions for rod pinch experiments

A pinhole camera with a 0.7 mm pinhole and an image plate was used to collect time-integrated images of the radiation pulses. The geometry of the pinhole imaging is shown in Fig. 19.

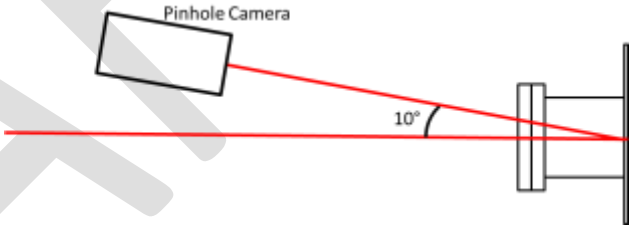

Figure 19 Pinhole camera geometry

B. Rod alignment

In these experiments, the designed radial diode gap on each rod was 0.635 cm. An initial concentricity check verified that on 9 of the10 rods, the minimum radial gap was 0.55 cm, and one rod had a minimum gap of 0.47 cm. The pinhole camera images and rod damage were approximately symmetric, so this degree of misalignment does not appear to have significantly affected the experiment.

IV. EXPERIMENTAL RESULTS

A. Electrical signals

The measured current for the 10 rod geometry described above, driven by this pulsed power configuration, is shown in Fig. 20. The current reaches a maximum value of about 145 kA at about 120 ns. The plotted current is the integral of the B-dot signal from location IE in Fig. 18. The plotted voltage is the inductively-corrected voltage from the V-dot at location IE in Fig. 18.

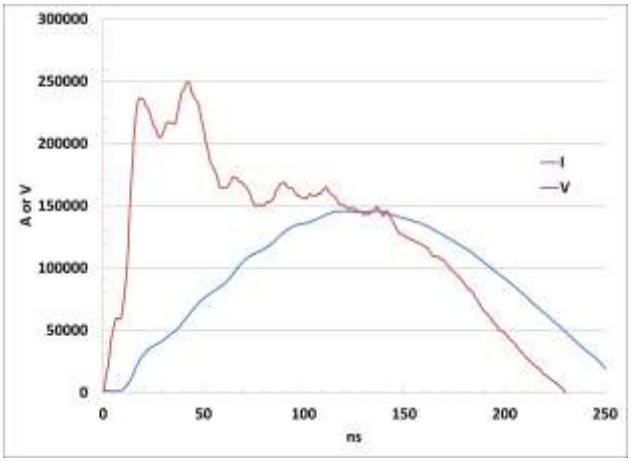

Figure 20 Current and voltage waveform for 10 rods with 0.635 cm radial A-K gap.

Inspection of the waveforms shows that the voltage initially rises steeply. The voltage has an initial peak about 20 ns after the start of the voltage pulse, and then drops for about 10 ns, after which it rises again, to peak about 45 ns after the start.

The current begins to flow when the voltage reaches about 60 kV, about 8 ns after the start of the voltage pulse. The rise time of the current is approximately 90 ns, and the fall time is similar.

The resulting impedance waveform is shown in Fig. 21. The impedance drops rapidly until about 70 ns, at which time it drops more slowly until the end of the pulse.

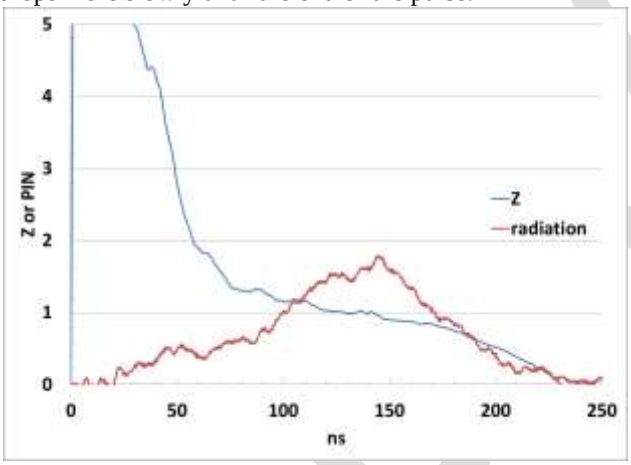

Figure 21 Impedance and radiation waveforms for 10 rods with 0.625 cm radial A-K gap.

B. Current division among the 10 rods

A first look at the current division among the 10 rods is provided by the x-ray pinhole image in Fig. 22. The rods are quite uniform in brightness, showing that the current division among the 10 rods was at least approximately symmetric.

Figure 22 Time-integrated x-ray pinhole image of the 10 rod array.

To evaluate the symmetry of current distribution through the 10 rod array, the current waveform measured by the rod Rogowski at each position can be compared to the total current measured by the B-dot located at position IE. Unfortunately, the Rogowki coil on the upper of the two center rods evidently was not functioning correctly, giving a current amplitude and pulse shape very different from that measured by the other center rod Rogowski and all the other current monitors, even though x-ray pinhole images and damage to the rod indicated that the current to that rod was very similar to that on the other rods. The current measured by the Rogowski on the other center rod was consistently 0.095-0.011 of the total current. Within the accuracy of the measurement, and neglecting the clearly anomalous reading of the other center rod Rogowski, the center rods carry the same current as the outer rods.

C. Current loss in the feed gap

The error in the initial setup of the feed gap, where it was set to 0.4 cm instead of 1.3 cm, provided an overtest of the design electric field in the gap. Fig. 23 shows the anode rod array after 8 shots. Note the white spot on the edge of each of the Rogowski coil holders, oriented toward the center of the array. This indicates the locations of current loss with this small feed gap machine configuration. The holders were not damaged, and were cleaned after the shot. When the feed gap was increased to 1.4 cm, these spots no longer appeared, and the loss across the gap to these locations appears to have stopped. Note also that there are no other spots on the anode, so no other regions of localized current loss are apparent.

Figure 23 Anode feed plate and rods after 8 shots.

D. *Effect of changing rod number*

The primary objective of this simulation and experimental program was to identify power loss and performance issues with large arrays of rod pinches, represented by the 10 rod array. However, other symmetric arrays of 8, 6, 4 and 2 rods, obtained by removing rods from the 10 rod array, were also tested.

Fig. 24 shows the PIN radiation signal for different rod numbers. The values for 10 and 8 rods are quite similar, rising later than for the other rod numbers, with the signal for 8 rods peaking substantially higher than for 10 rods. The signal for 6 rods rises earlier and more rapidly, and continues to rise until 120 ns, peaking with the largest signal of any rod number. The signals for 4 rods rise similarly to 6 rods until about 100 ns, at which time they plateau, beginning to drop at 120 ns. The signal for 2 rods rises much earlier and more steeply than for the larger rod numbers, but peaks early, at 70 ns, and then drops more rapidly.

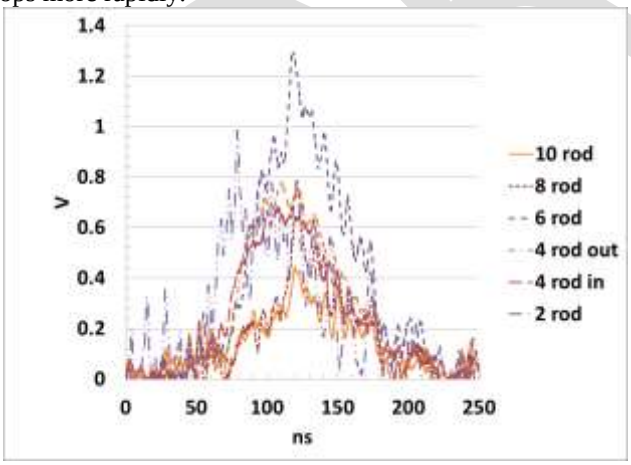

Figure 24 PIN signal vs. rod number.

Fig. 25 shows the coupled power computed from the voltage and current waveforms for different rod numbers. The values for 10 and 8 rods are very similar, while when the rod number decreases to 6 the coupled power increases by about 30%. As the rod number is decreased to 4, the coupled power increases another 10 to 20%. As the rod number drops to 2 the coupled power begins to drop. Note that the radiation signal recorded by the PIN does not track the coupled power very closely. This is likely because of the geometric complexity of the radiation source region, which includes the sides of the anode rods under the cathode and the end of the rod. The location of the radiation source within this geometry probably changes during the pulse, moving from the area under the cathode early in the pulse toward the end of the rod later in the pulse.

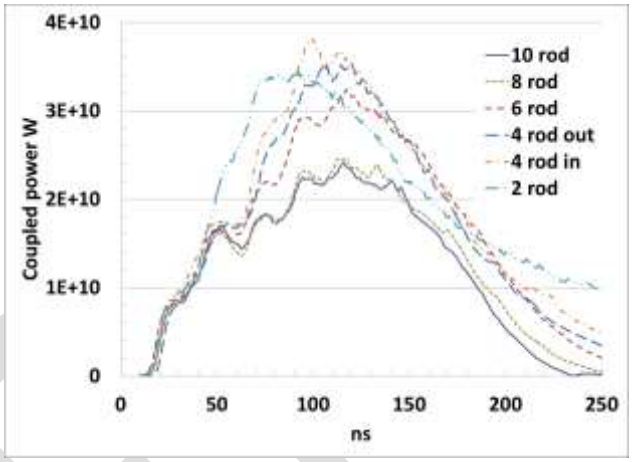

Figure 25 Coupled power vs. rod number.

Fig 26 shows pinhole x-ray images of the 8 rod, 6 rod, 4 rod in, and 4 rod out configurations. In all cases the power division among the rods appears to be very even, and the pinches as slightly biased towards the center of the array, as in the 10 rod case. Inspection of the feed gap during this set of shots showed no indications of current loss to the rod Rogowskis or other points in the feed gap. Even at the peak voltage of greater than 500 kV observed in the 2 rod configuration, no feed losses were observed.

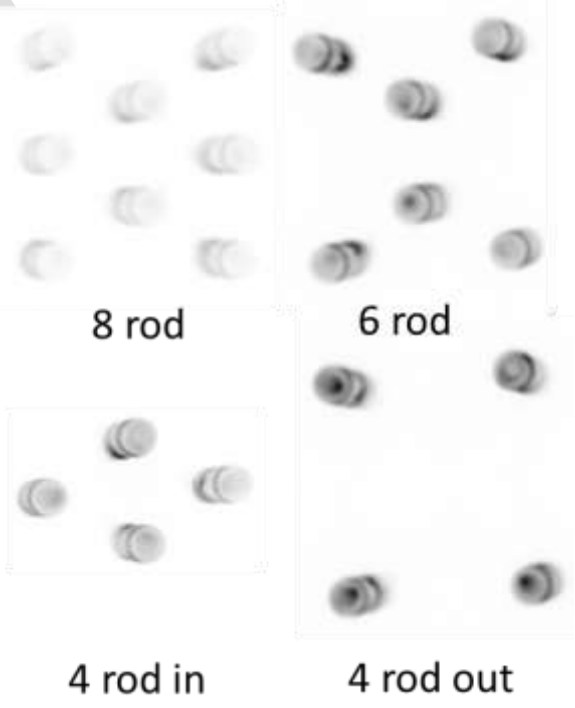

Figure 26 Time-integrated pinhole images of rod pinch arrays containing eight, six, and two configurations of four rods.

V. Discussion

Overall generally good agreement was observed between the simulations and experiments for this geometry.

A. Current and voltage behavior

The current and voltage in Fig. 20 can be compared with the simulated current in Fig. 11 and the simulated voltage in Fig 12. The currents differ substantially, with the measured current peaking at about 150 kA while the simulated current reached 300 kA. At the same time, the simulated and measured voltages are more similar, with the simulated voltage peaking at about 170 kV while the measured voltage has an early peak of 250 kV, and is about 150 kV near the peak current. In addition, the measured current rise time of about 90 ns is much longer than the simulated rise time of about 50 ns. These effects might be attributed to impedance mismatch between the LTD driver and the load.

In previous single rod experiments using the same pulsed power driver, a single rod with a small A-K gap was a 3 ohm load, and the measured current and voltage waveforms are shown in Fig. 27. This behavior is roughly similar to that observed with the 10 rod array in Fig. 20, with a peak power of 3 x 10^{10} W at about 100 ns, compared to a measured 2.2 x 10^{10} W at 120 ns for the array. These can be contrasted with a simulated 5.1 x 10^{10} W at 90 ns for the array. Evidently the driver cannot supply the full current for this undermatched load.

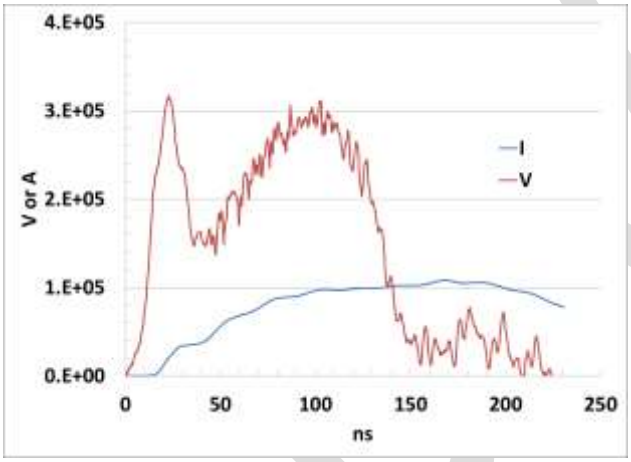

Figure 27 Current and voltage waveforms for a single tungsten anode, radius 1.27 cm with a 1.6 cm cathode radius.

B. Impedance behavior

Measured and fitted impedance waveforms for the 10 rod array are shown in Fig. 28. The falling impedance is fitted using a gap closure velocity of 0.5 cm/μs. This can be contrasted with the calculated diode impedance in Fig. 14, which does not include gap closure effects. As noted in the simulation discussion before Fig. 16, pinching effects are expected to be weak, and the bulk of the flow is near the anode-cathode gap.

Figure 28 Measured and fitted impedance waveforms for the 10 rod array. The fit assumes no ions in the gap and a cathode plasma gap closure velocity of 0.5 cm/μs.

C. Coupling to the LTD driver

The power coupled from the driver to the rod pinch array is maximized for the 4 rod configurations, as shown in Fig. 25. These configurations operate at 3 to 3.5 ohms impedance during the impedance plateau between 70 and 200 ns. Coupled power is reduced for arrays with larger numbers of rods. Comparison with the simulations shows this is largely because the driver cannot supply the current to these low impedance loads. Coupled power is also reduced for the 2 rod load, which operates at about 8 ohms. As expected, efficient power coupling to a load consisting of an array of rod pinches requires that the driver impedance be matched to the load.

D. Asymmetry in the rod pinch flow

Simulations clearly show that in a closely coupled array of small aspect ratio rod pinch diodes, the flow in the A-K gap is asymmetric, with smaller magnetic fields on the side facing the center of the array, as seen in Fig. 13. This effect can also be seen in x-ray images of the array, such as Fig. 22, with darker spots indicating higher current density on the side of the rods facing the center of the array. However, as seen in the x-ray image, the asymmetry in the flow is not large, and impedance calculations neglecting this asymmetry give good agreement with experiments, as in Fig. 28.

E. Comparison of experimental results with simulation results

It is worth noting that the rod voltages as seen in Fig. 12 are in excellent agreement with one another despite the stair-step nature of the conductor surfaces in the rod-hole regions. The electric fields in the simulation are comparable from rod to rod suggesting that the simulation model is acceptable in cases where the rods are not perfectly centered on axis.

For the simulation shown in Fig. 15, no electron deposition or ion emission was found on or near the Rogowski coil holders. This finding agrees with experimental results that show no damage to those hardware components. Note that little electron emission occurs from the upstream side of the cathode cans, emission points that previous simulations show are the largest sources of electrons that strike the anode rod holders. The Rogowski coil housings do not undergo high

enough levels of Ohmic heating to result in ion emission without the added energy of electrons striking their surfaces. The 3 mm rod AK gap setting successfully eliminates undesirable ion emission from the Rogowski coil holders.

A comparison of simulated energy deposition on anode rod 4 as shown in Fig. 16 and the experimental x-ray image in Fig. 22 shows good agreement. In both cases a dark band near the cathode is visible indicating an area of high current density, and a weaker band is visible around the edge of the end of the rod.

The early-time, high-voltage (approximately 240 kV) feature seen in the experimental data in Fig. 20 was seen in earlier simulations that had larger AK gaps of approximately 7 mm. However, once the AK gaps were set to match experimental settings and the drive voltage set accordingly, this early-time feature was lost. The fact that this early time high voltage feature was present in the large gap simulation but absent in the small gap simulation, suggests that it may result from delayed turn on of the diode in the weaker electric field in the large gap simulation. The fact that this feature is present in the experiments therefore suggests that the initial electric field in the experiments was too low to promptly turn on the cathode emission. Careful attention to getting high enough fields to promptly turn on cathode emission in these large parallel rod pinch arrays is required.

VI. Conclusion

Large arrays of rod pinches may be useful loads for low impedance pulsed power drivers. However, coupling of the load to the interior of the array, power losses due to magnetic nulls in the feeds, and asymmetry in the rod pinch flow in the presence of the overall magnetic field of the array are concerns for the performance of these rod pinch arrays.

Experiments with a closely coupled, small aspect ratio ten rod pinch array, and simulations which are in good agreement with experiment, show that coupling of the power to the interior of the array does not appear to be a problem. The central rods appear to carry almost exactly the same current as the rods on the periphery of the array. Power losses in the feed are observed with very small feed gaps, but control of the feed gap electric field allows operation without these losses. Asymmetry in the rod pinch power flow is observed, but does not appear to have deleterious effects on the operation of the array.

Two areas of particular concern are design of the feed gap geometry to avoid electron emission from the cathode plate away from the rod gaps, and design of the cathode at the rod gap to insure prompt initiation of electron flow in the rod gap.

Acknowledgment

The authors would like to thank Bryan Oliver for his encouragement of this research, and for many useful discussions. The crew of Ursa Minor provided outstanding support for these experiments.

References

[1] R. A. Mahaffey, J. Golden, Shyke A. Goldstein, and G. Cooperstein, "Intense electron beam pinch formation and propagation in rod pinch diodes," *Appl. Phys. Lett.*, vol. 33, no. 9, pp. 795-797, Nov, 1978.

[2] G. Cooperstein, J. R. Boller, R. J. Commisso, D. D. Hinshelwood, D. Mosher, P. F. Ottinger, J. W. Schumer, S. J. Stephanakis, S. B. Swanekamp, B. V. Weber, F. C. Young, "Theoretical modeling and experimental characterization of a rod-pinch diode", *Phys. Plasmas* vol. 8, no. 10, pp. 4618-4636, Oct. 2001; S. B. Swanekamp, G. Cooperstein, J. W. Schumer, D. Mosher, F. C. Young, P. F. Ottinger, R. J. Commisso, "Evaluation of self-magnetically pinched diodes up to 10 MV as high-resolution flash X-ray sources," *IEEE Trans. Plasma Sci.* vol. 32, no. 5, pp. 2004-2016, Oct. 2004; R. J. Commisso, G. Cooperstein, D. D. Hinshelwood, D. Mosher, P. F. Ottinger, S. J. Stephanakis, S. B. Swanekamp, B. V. Weber, F. C. Young, "Experimental evaluation of a megavolt rod-pinch diode as a radiography source," *IEEE Trans. Plasma Sci.* vol. 30, no. 1, pp. 338-351, Feb. 2002; F. Young, R. J. Commisso, R. J. Allen, D. Mosher, S. B. Swanekamp, G. Cooperstein, F. Bayol, P. Charre, A. Garrigues, C. Gonzales, F. Pompier and R. Vezinet, "Rod-pinch diode operation at 2 to 4 MV for high resolution pulsed radiography," *Phys. Plasmas* vol. 9, no. 11, pp. 4815, Nov. 2002; P. R. Menge, D. L. Johnson, J. E. Maenchen, D. C. Rovang, B. V. Oliver, D. V. Rose and D. R. Welch, "Optimization of a rod pinch diode radiography source at 2.3 MV," *Rev. Sci. Instrum*. Vol. 74, no. 8, pp. 3628-3635, Aug. 2003; B. Etchessahar, Virgile Bernigaud, Michel Caron, Frédéric Cartier, Stéphanie Cartier, Laurent Hourdin, Laurent Magnin4, Rémi Nicolas, Frédéric Poulet, Rodolphe Rosol, Yaël Tailleur, Martial Toury, Antoine Compant La Fontaine, Béatrice Bicrel, Bruno Cassany, Thierry Desanlis, Luc Voisin, David Hébert, Christophe Delbos, Alain Garrigues and Isabelle Soleilhavoup, "Study and optimization of negative polarity rod pinch diode as a flash radiography source at 4.5 MV," *Phys. Plasmas* vol. 19, no. 9, pp. 093104, Sep. 2012; C. L. Miller, D. R. Welch, D. V. Rose and B. V. Oliver, "Detailed simulation of the CYGNUS rod pinch radiographic source," *IEEE Trans. Plasma Sci.* vol. 38, no. 10, pp. 2507-2513, Oct. 2010; Yi Gao1, Aici Qiu, Zhong Zhang, Pengfei Zhang, Zhiguo Wang and Hailiang Yang, "Research on pinching characteristics of electron beams emitted from different cathode surfaces of a rod-pinch diode," *Phys. Plasmas* vol. 17, no. 7, pp. 073108 July 2010.

[3] B. V. Oliver, P. F. Ottinger, T. C. Genoni, J. W. Schumer, S. Strasburg, S. B. Swanekamp, and G. Cooperstein, " Magnetically insulated electron flow with ions with application to the rod-pinch diode", *Phys. Plasmas* vol. 11, no. 8, pp. 3976-3991, Aug. 2004.

[4] B. V. Weber, R. J. Commisso, G. Cooperstein, D. D. Hinshelwood, D. Mosher, P. F. Ottinger, D. M. Ponce, J. W. Schumer, S. J. Stephanakis, S. D. Strasburg, S. B. Swanekamp, and F. C. Young, "Ultra-high electron beam power and energy densities using a plasma-filled rod-pinch diode", *Phys. Plasmas* vol. 11, no.2, pp. 2916-2927, May, 2004.

[5] V. J. Harper-Slaboszewicz, J. Leckbee, P. W. Lake, A. L. McCourt, "Effect of Rod Material on the Impedance Behavior of Small Aspect Ratio Rod Pinches", *IEEE Trans. Plasma Science*, 2014.

[6] J. Leckbee, S. Cordova, B. Oliver, T. Webb, M. Toury, M. Caron, R. Rosol, B. Bui, T. Romero, D. Ziska, "Linear Transformer Driver (LTD) Research for Radiographic Applications," in *Proceedings of the IEEE Pulsed Power Conference*, 2011, pp.614-619.

[7] T. D. Pointon, W. A. Stygar, R. B. Spielman, H. C. Ives, and K. W. Struve, "Particle-in-cell simulations of electron flow in the post-hole convolute of the Z accelerator", *Phys. Plasmas* vol. 8, no. 10, pp. 4534-4544, Oct. 2001; D. V. Rose, D. R. Welch, T. P. Hughes, R. E. Clark, and W. A. Stygar, "Plasma Evolution and Dynamics in High-Power Vacuum-Transmission-Line Post-Hole Convolutes," *Physical Review Special Topics-Accelerators and Beams*, vol. 11, 2008, pp. 1-10.

[8] D. R. Welch, D. V. Rose, M. E. Cuneo, R. B. Campbell, and T. A. Mehlhorn, "Integrated simulation of the generation and transport of proton beams from laser-target interation," *Phys. Plasmas* 13, 063105 (2006).

[9] J. A. Halbleib, R. P. Kensek, G. D. Valdez, S.M. Seltzer, and M. J. Berger, "ITS: the integrated TIGER series of electron/photon transport codes - Version 3.0," *IEEE Trans. Nucl. Sci*. 39, 1025 (1992).

[10] D. V. Rose, D. R. Welch, B. V. Oliver, R. E. Clark, D. L. Johnson, J. E. Maenchen, P. R. Menge, C. L. Olson, and D. C. Rovang, "Coupled particle-in-cell and Monte Carlo transport modeling of intense radiographic sources," *J. Appl. Phys*. 91, 3328 (2002).

[11] M. S. Di Capua and D. G. Pellinen, "Propagation of power pulses in magnetically insulated vacuum transmission lines," *J. Appl. Phys.* 50, 3713 (1979).

[12] T. W. L. Sanford, J. A. Halbleib, J. W. Poukey, A. L. Pregenzer, R. C. Pate, C. E. Heath, R. Mock, G. A. Mastin, D. C. Ghiglia, T. J. Roemer, P. W. Spence, and G. A. Proulx, "Measurement of electron energy deposition necessary to form an anode plasma ta, ti and c for coaxial bremsstrahlung diodes," *J. Appl. Phys.* 66, 10 (1989).

[13] R. K. Parker, R. E. Anderson, and C. V. Duncan, "Plasma-induced field emission and the characteristics of high-current relativistic electron flow," *J. Appl. Phys.*, vol. 45, no. 6, pp. 2463–2479, June, 1974.

[14] D. D. Hinshelwood, "Explosive emission cathode plasmas in intense relativistic electron beam diodes," Naval Research Laboratory, Washington, DC, NRL Memo. Rep. 5492, Jan. 1985.